

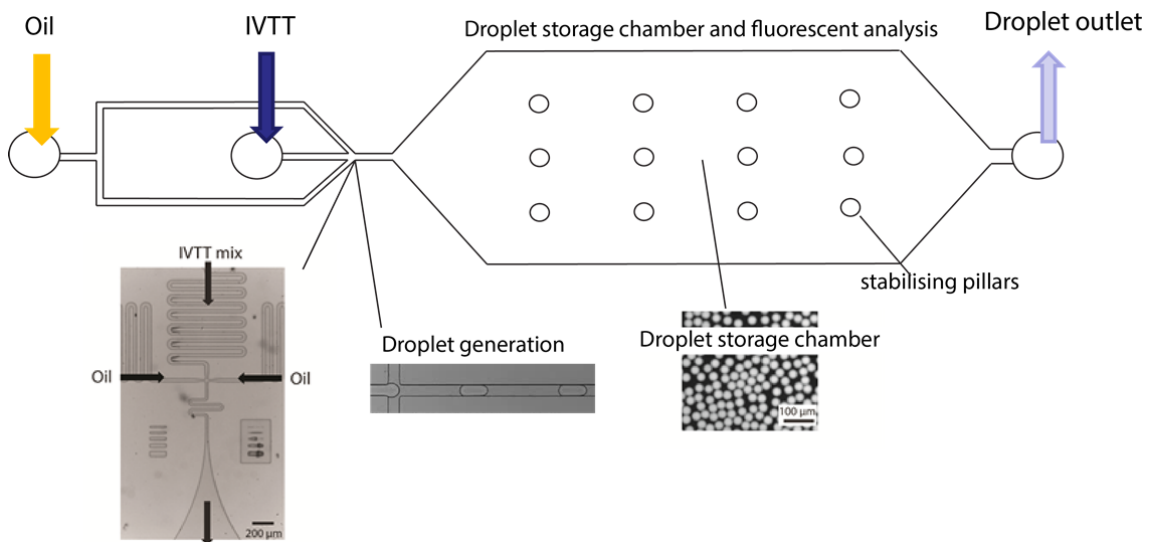
## Macromolecular crowding develops heterogeneous environments of gene expression in picoliter droplets

Maike M. K. Hansen, Lenny H. H. Meijer, Evan Spruijt, Roel J. M. Maas, Marta Ventosa Roquelles, Joost Groen, Hans A. Heus, Wilhelm T. S. Huck

### Supplementary information

#### Supplementary figures

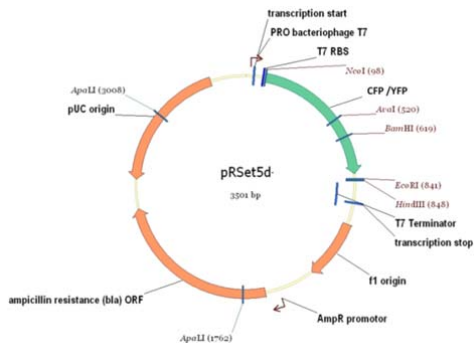
Supplementary Fig. 1



Drawing of the PDMS-based microfluidic chip. Two inlets including one for the oil and one for the *in vitro* transcription and translation mix (IVTT). Droplets are generated using PDMS based microfluidic chips, the IVTT mixture is pinched off at regular intervals by oil generating monodisperse water in oil emulsions. The droplets are stored in the storage chamber and can be monitored over time with fluorescence microscopy.

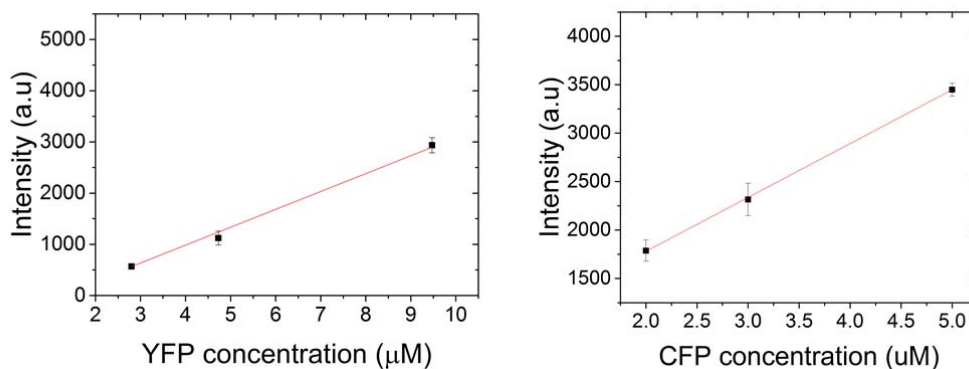
Supplementary Fig. 2

Plasmid map of pRSET-CFP/ YFP (see Methods section for more details).



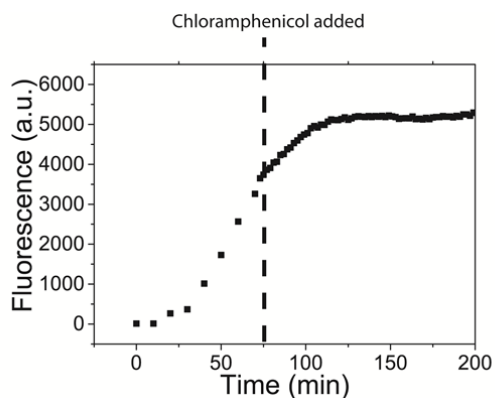
### Supplementary Fig. 3

Calibration curves CFP and YFP (Bio Vision). By measuring the fluorescent intensity at known protein concentrations we could determine the protein concentrations produced in our experiments.



### Supplementary Fig. 4

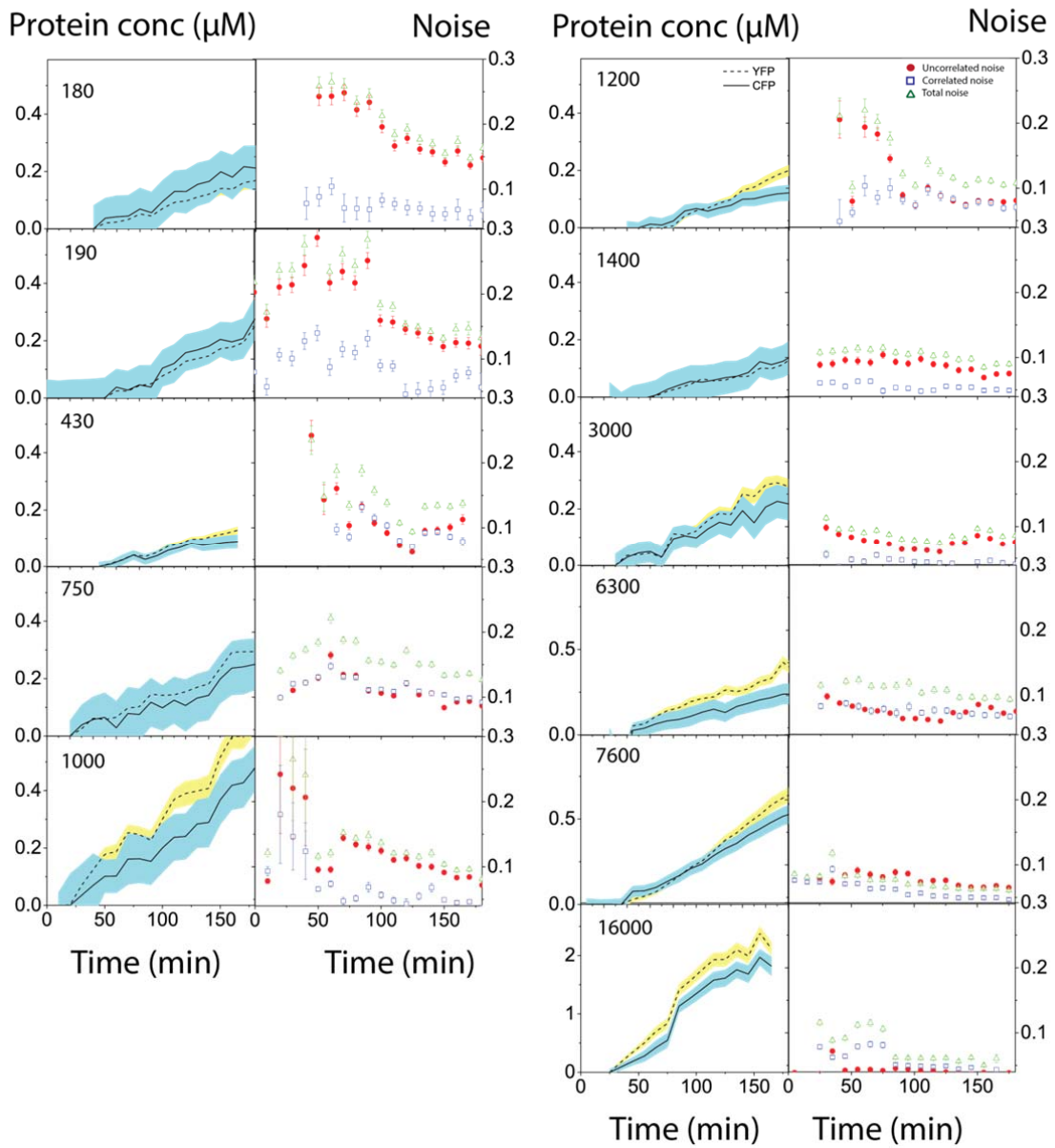
Cell free protein expression was performed in bulk (50 μL) at 30°C. Addition of chloramphenicol after 75 minutes of CFP expression, results in an additional increase in fluorescence due to residual maturation of the protein. Subsequently there is no decrease in fluorescent intensity for the following 100 minutes. Due to the addition of chloramphenicol we have no additional protein production, and since the fluorescent signal stays constant we can assume there is no protein degradation within our measuring time.



### Supplementary Fig. 5

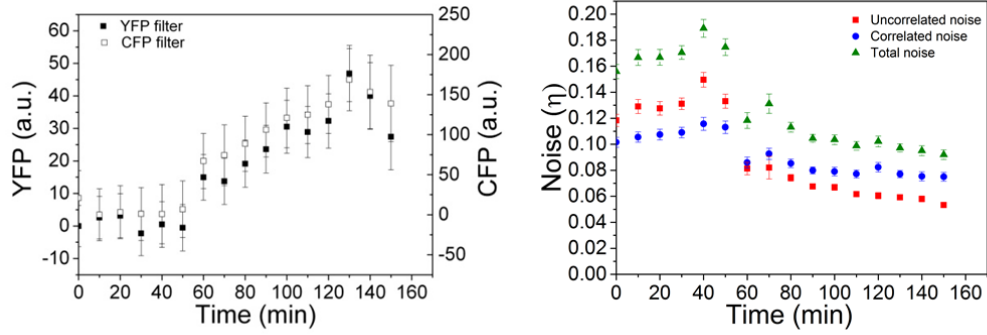
Expression and noise curves of images from Figure 3a. Average CFP (full line) and YFP (dotted line) expression over all droplets with standard deviation in blue and yellow respectively. Uncorrelated (red full squares), correlated (blue empty circles) and total noise (green empty triangles) values over time.

# Dilute



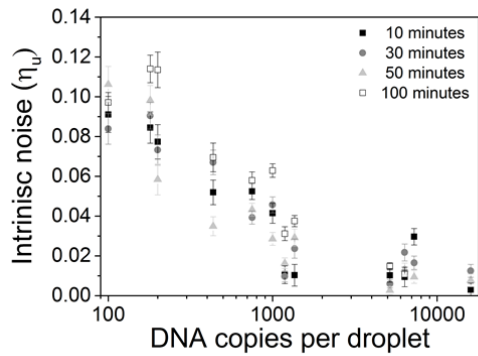
**Supplementary Fig. 6**

GFP was expressed from pRSET-GFP under the YFP and CFP filter. After the initial lag phase of 50 minutes the protein expression starts and can be measured under both CFP and YFP filter. Uncorrelated, correlated and total noise can be calculated for one protein, meaning that any calculated uncorrelated noise comes from imaging and analysis, since the detection of one protein under two filters should give no uncorrelated noise.



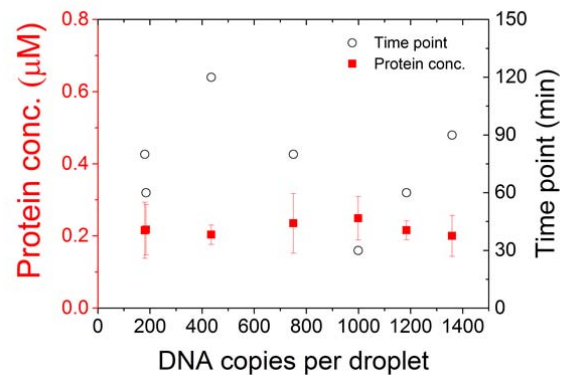
**Supplementary Fig. 7**

We subsequently subtracted the uncorrelated noise due to imaging and analysis (Fig. 2) from uncorrelated noise values at 10, 30, 50 and 100 minutes after the start of fluorescence increase for the range of DNA concentrations tested. This shows that the same trend is visible at all four time points with all time-points tending to 0 with increasing copy number.

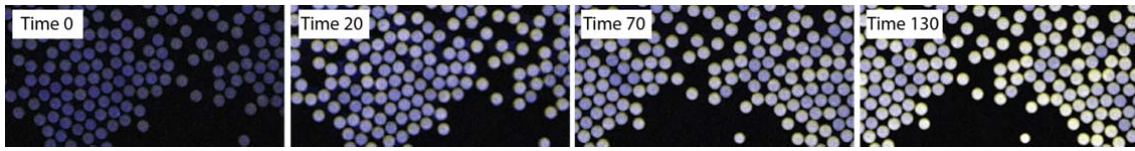


**Supplementary Fig. 8**

Using the calibration curves shown in Fig. 3 we chose time points at which the total CFP and YFP concentration per droplet averaged over the whole population of droplets was approximately  $0.2 \mu\text{M}$ . The graph shows the time points (open black circle) and protein concentration (closed red square) chosen for the range of DNA concentrations.



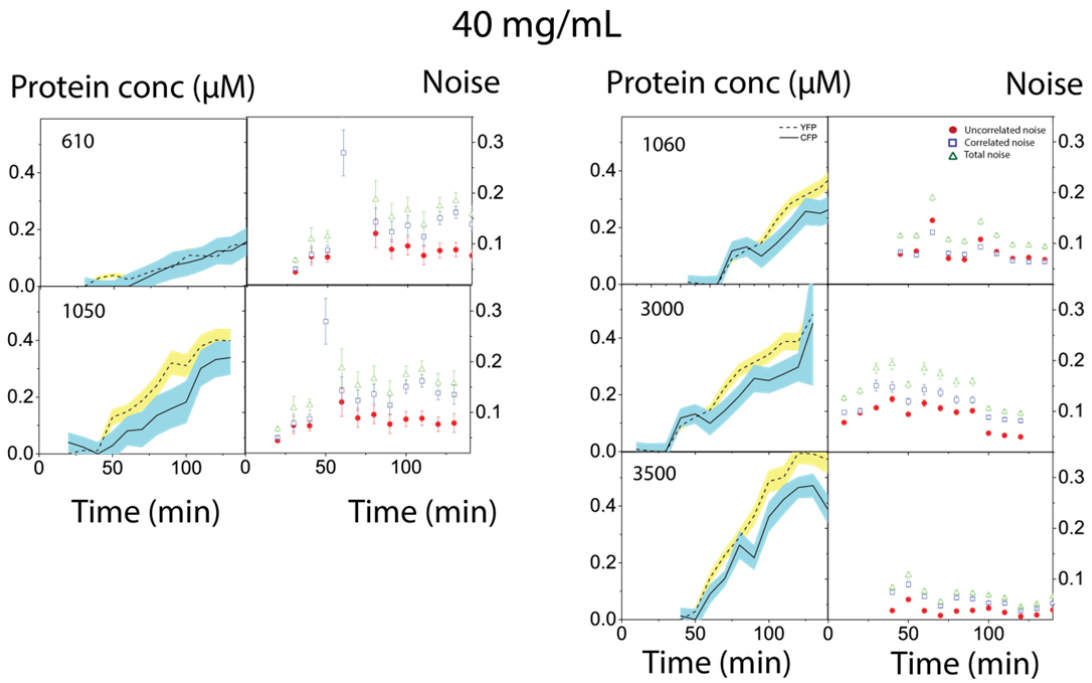
### Supplementary Fig. 9



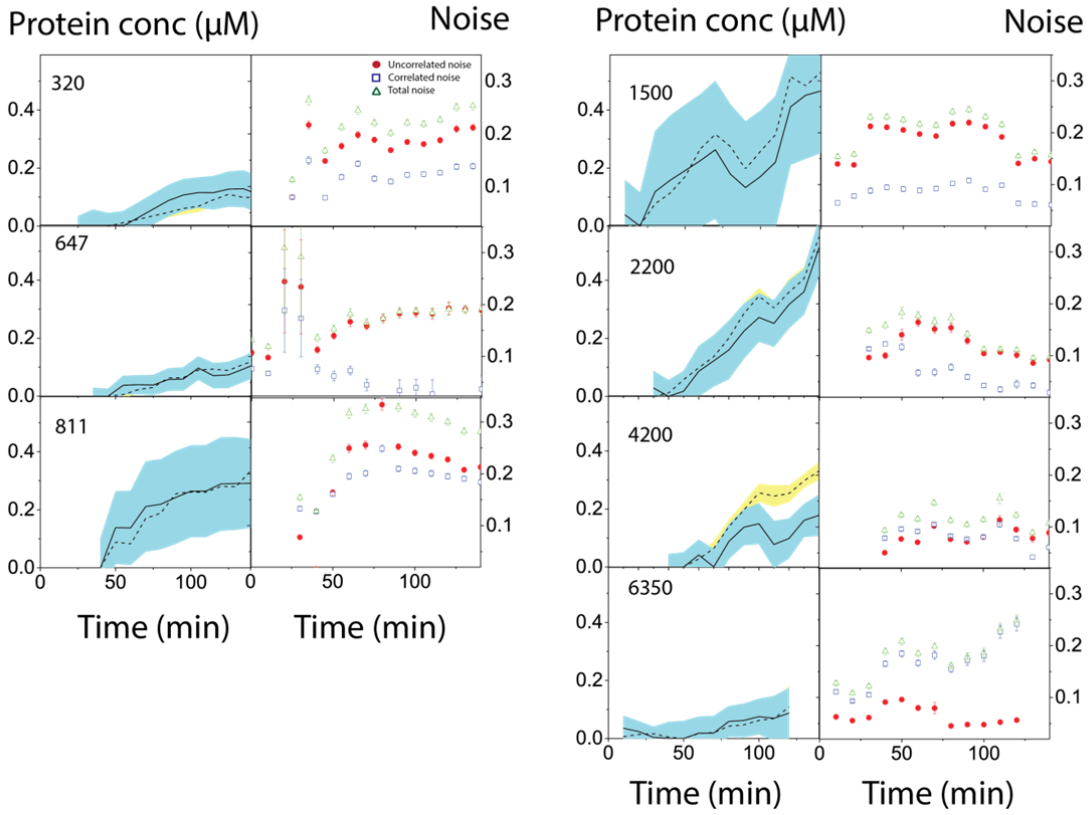
Time course of expression in the presence of  $90 \text{ mg mL}^{-1}$  Ficoll 70 for 600 copies of CFP and YFP plasmid per droplet.

### Supplementary Fig. 10

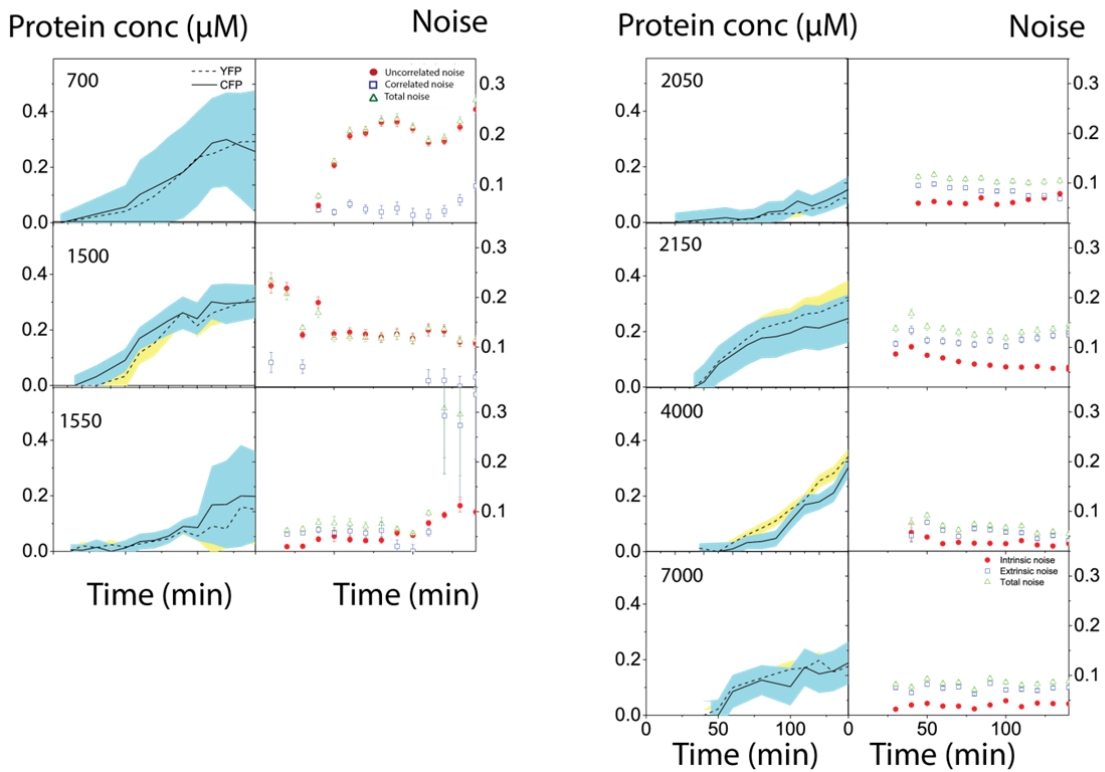
Expression and noise curves over time for 40 70 and 90  $\text{mg mL}^{-1}$  Ficoll 70. Average CFP (full line) and YFP (dotted line) expression over all droplets with standard deviation in blue and yellow respectively. Uncorrelated (red full squares), correlated (blue empty circles) and total noise (green empty triangles) values over time.



### 70 mg/mL

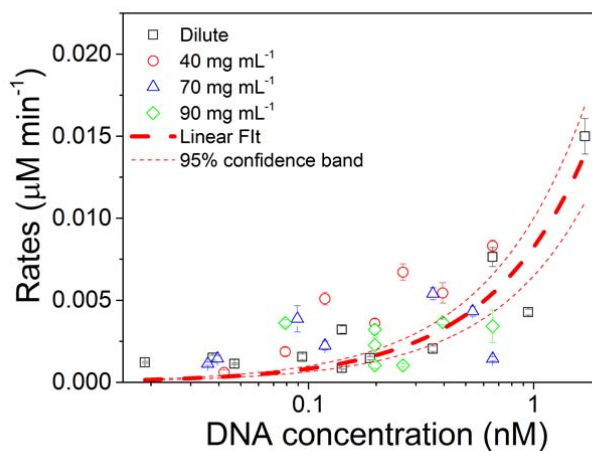


### 90 mg/mL

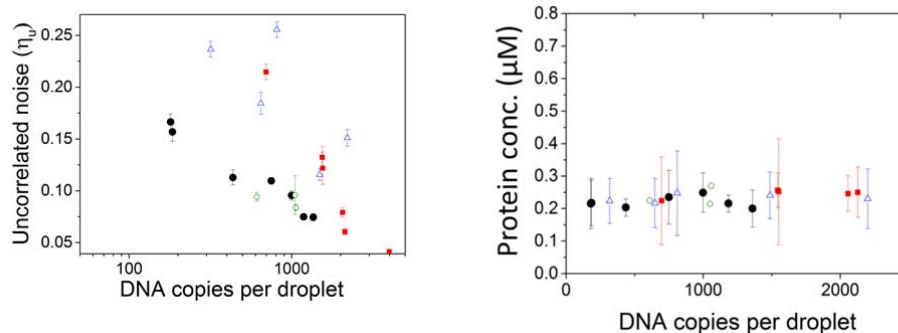


### Supplementary Fig. 11

YFP expression rate corresponding to the CFP expression rates shown in Fig. 4a; 0 mg mL<sup>-1</sup> Ficoll in black square, 40 mg mL<sup>-1</sup> Ficoll in green diamond, 70 mg mL<sup>-1</sup> Ficoll in blue triangle and 90 mg mL<sup>-1</sup> Ficoll in red circle, error bars represent the standard error of the fitting the linear part of the protein expression curve. Red dashed line is linear fit for 0 mg mL<sup>-1</sup> showing 95% confidence bands



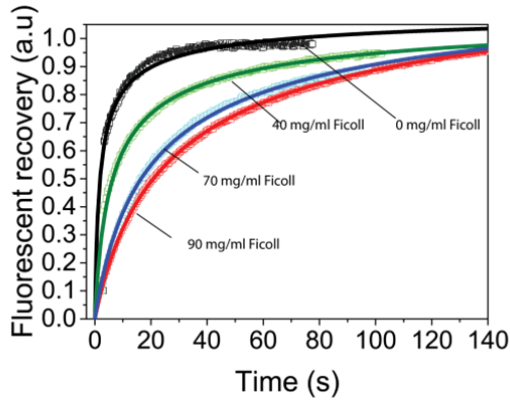
### Supplementary Fig. 12



Uncorrelated noise values for a DNA plasmid copy number range (left) at different time points where the total protein produced was 0.2 nM, at different Ficoll 70 concentrations, 0 mg mL<sup>-1</sup> in black full circle, 40 mg mL<sup>-1</sup> in green empty circle, 70 mg mL<sup>-1</sup> in blue empty triangle and 90 mg mL<sup>-1</sup> in red full square. Error bars show 95% confidence intervals, which were calculated by bootstrapping from the original distribution. Using the calibration curves shown in Fig. 3 we chose time points at which the total CFP and YFP concentration per droplet averaged over the whole population of droplets was approximately 0.2 nM. Protein concentrations are shown on the right, 0 mg mL<sup>-1</sup> in black full circle, 40 mg mL<sup>-1</sup> in green empty circle, 70 mg mL<sup>-1</sup> in blue empty triangle and 90 mg mL<sup>-1</sup> in red full square.

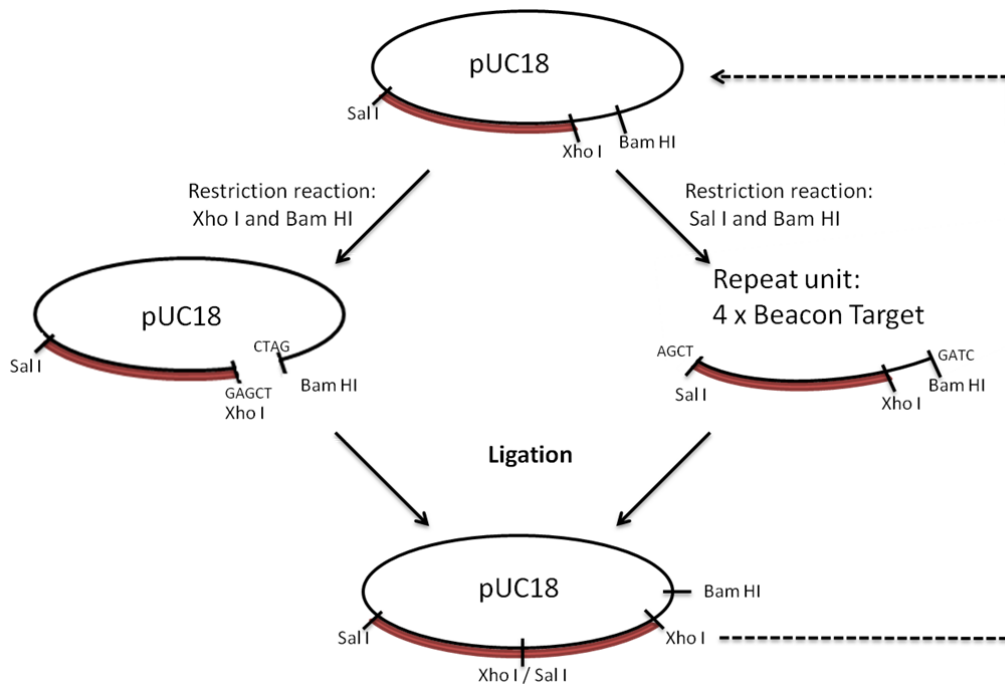
### Supplementary Fig. 13

Fluorescence recovery after photo-bleaching of Alexa 647 labelled ribosomes, dilute in black, 40 mg ml<sup>-1</sup> Ficoll in green, 70 mg ml<sup>-1</sup> Ficoll in blue and 90 mg ml<sup>-1</sup> Ficoll in red. Fittings are performed with the Ellenberg Diffusion Fitting.



### Supplementary Fig. 14

Formation of 32 x Beacon target.

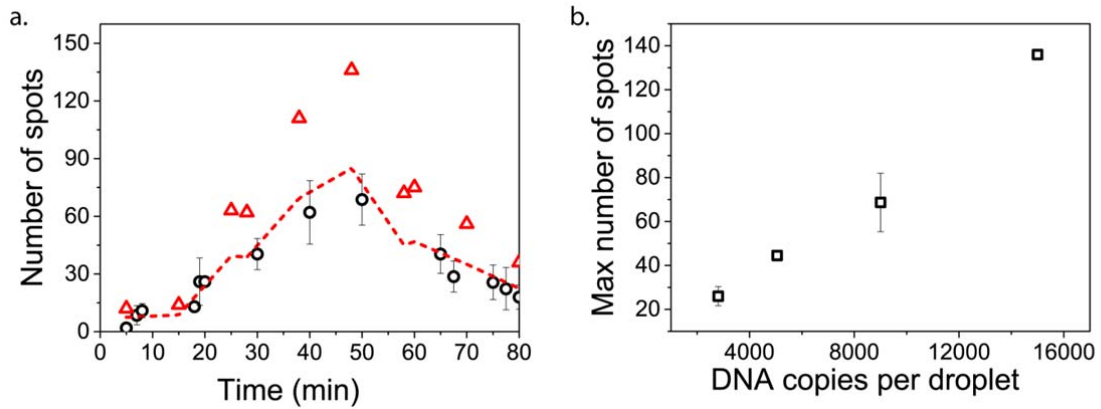


Scheme showing the procedure for cloning the 32 X Beacon target, after the first insertion of an oligonucleotide containing four repeat units, the target region (marked in red) was cut out with *SalI* at the 5' end of the coding sequence (CDS) and *BamHI* at the 3' end of the CDS. The plasmid backbone also containing the target region was cut with *XhoI* and *BamHI* both at the 3' end of the CDS, this was ligated with *BamHI* since *XhoI* and *SalI* have complementary sticky ends. The resulting plasmid was



subsequently amplified in Top 10 cells. This procedure was repeated until a 32 x Repeat unit was formed.

**Supplementary Fig. 15**



The black circles in Fig S15a correspond to the same data as shown in Fig. 5b in the main text. The red triangles are the number of spots detected in a different experiment with a higher DNA copy number. When correcting for the copy number the red dashed line clearly lies within the standard deviations of the black circles. We therefore analysed 4 different copy numbers and plotted the maximum number of spots for each (Fig. 15b) this shows a clear linear correlation, the squares are averages of a minimum of 2 droplets and the error bars are resulting standard deviations.

**Supplementary Fig. 16**

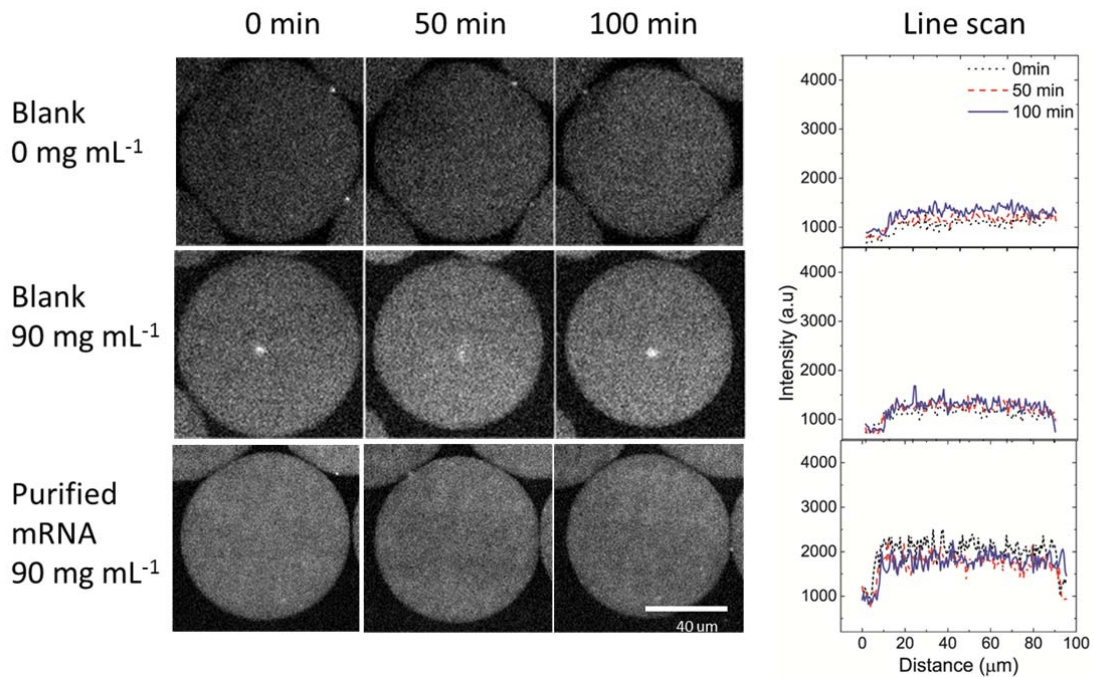
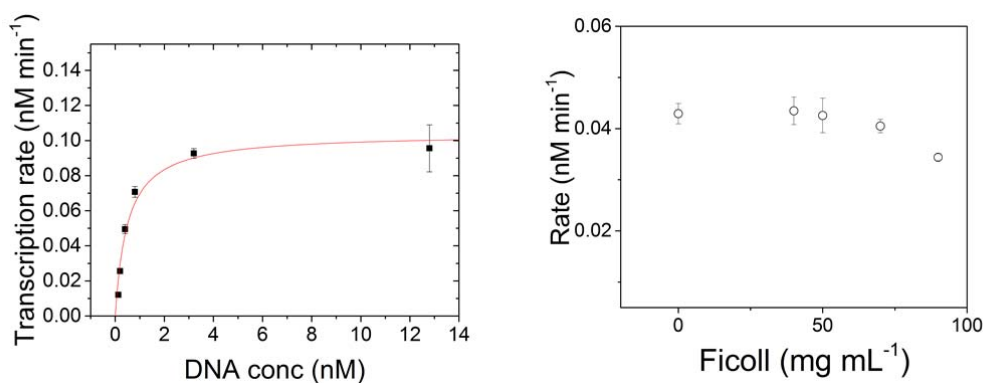


Figure S15 shows blanks in the absence of Ficoll and in the presence of 90 mg mL<sup>-1</sup> of Ficoll over time. The graphs show corresponding line scans. All three remain at more or less the same intensity over time. Furthermore, the images do not show any bright spots appearing indicating that the spots are not an aggregation of the molecular beacon in the presence of Ficoll. For the purified mRNA we used (4.4 nM) which was estimated (Supplementary Fig. 16) to be the mRNA concentration produced after 100 minutes). The line scans show no background subtractions.

### Supplementary Fig. 17

Transcription was determined experimentally using Michaelis-Menten fitting, resulting in a typical  $K_m$  of 0.5 nM and  $V_{max}$  of 0.1 nM min<sup>-1</sup>. The graph on the left shows the Michaelis-Menten fit (red) of mRNA production rates experimentally determined (black) with error bars indicating the standard error of the fitting to the linear part of the expression curves. The graph on the right shows that the mRNA production rate does not substantially change with different Ficoll concentrations. Therefore we used the same  $K_m$  and  $V_{max}$  values for all Ficoll concentrations. The mRNA production rates were measured with a DNA concentration of 0.6 nM and using the transcription only the method as described in Supplementary methods. The rate was taken as a linear fit to the linear part of the mRNA expression curve with error bars indicating the standard error of the fitting.



### Supplementary Fig. 18

Diffusion coefficients of polysomes with increasing Ficoll concentrations were calculated using the fitting obtained from the diffusion coefficients of ribosomes. The diffusion coefficient of the polysome at 0 mg mL<sup>-1</sup> Ficoll was calculated using Stokes-Einstein Equation, assuming an average end to end distance of 76 nm. Which was calculated from equation 1:

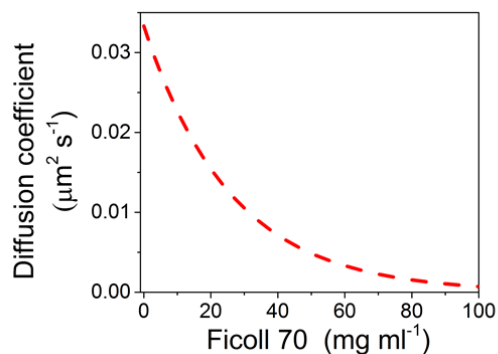
$$\langle r^2 \rangle_0 = 2 a L_c \left(1 - \frac{a}{L_c}\right)$$

Where  $\langle r^2 \rangle_0$  is the average squared end-to end distance of the polymer,  $a$  its persistence length and  $L_c$  its contour length. ( $L_c = 0.59$  nm/nucleotide,  $a = 5$  nm).

Subsequently the decrease in diffusion coefficient due to the formation of the polysome, with an average distance of 22 nucleotides<sup>1</sup> between ribosomes ( $2.3 \times 10^6$  Da)<sup>2</sup> on the mRNA transcript, was calculated from:

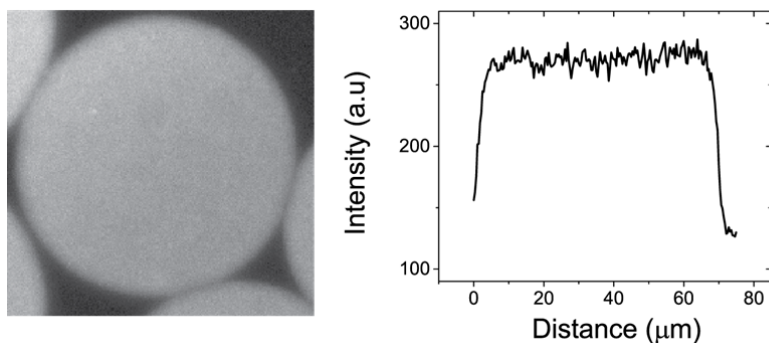
$$f \propto M^{\frac{1}{2}}$$

The resulting calculated diffusion coefficients of polysomes in Ficoll are shown in the graph below.



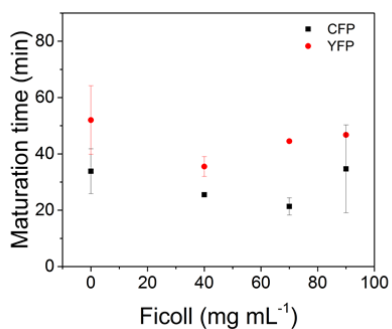
### Supplementary Fig. 19

Fluorescein labelled pRSET-CFP and pRSET-YFP (0.6 nM total) showing homogeneous DNA distribution in the presence of 90 mg mL<sup>-1</sup> of Ficoll 70.



### Supplementary Fig. 20

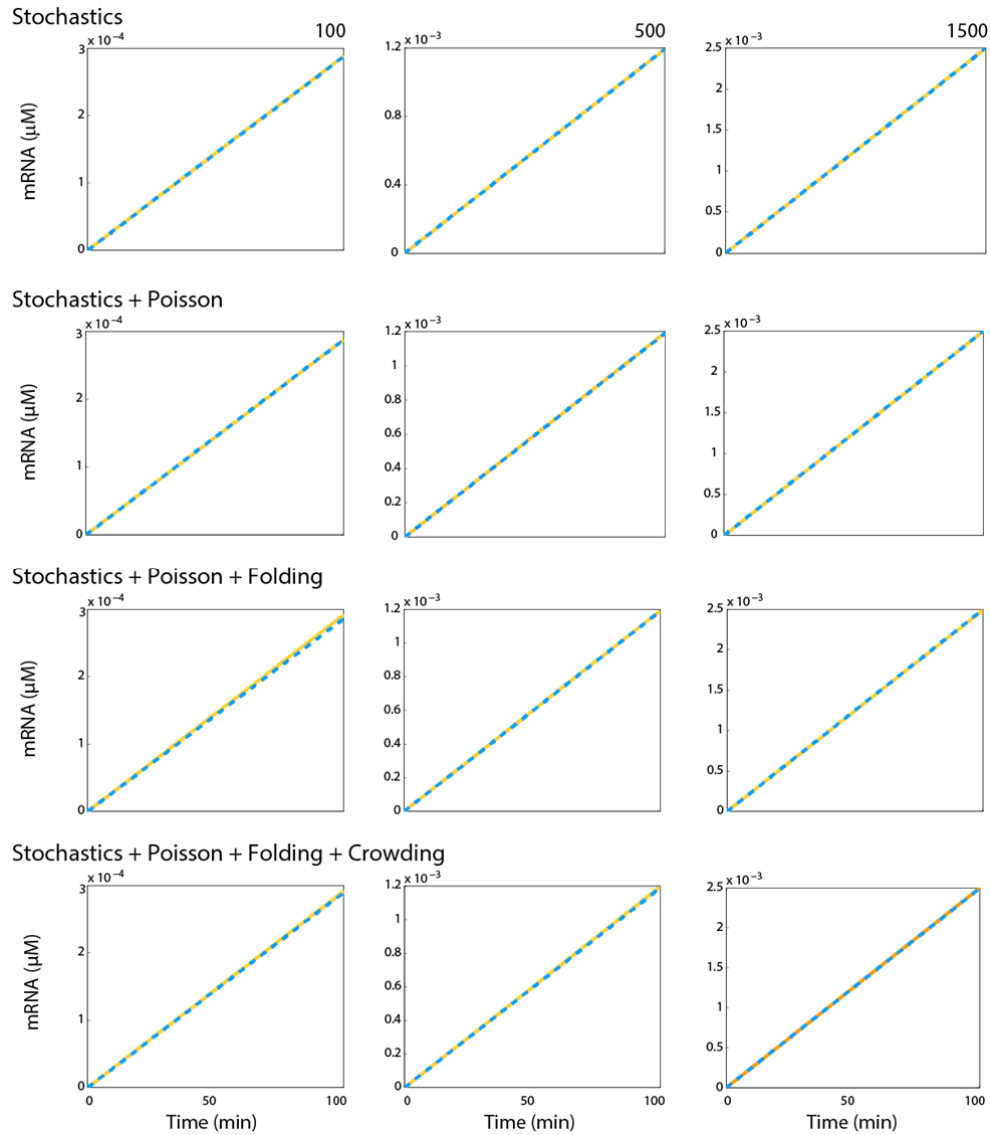
Effect of Ficoll 70 on maturation times of CFP (black full square) and YFP (red full circle). Error bars denote are calculated from multiple measurements.



## Supplementary Fig. 21

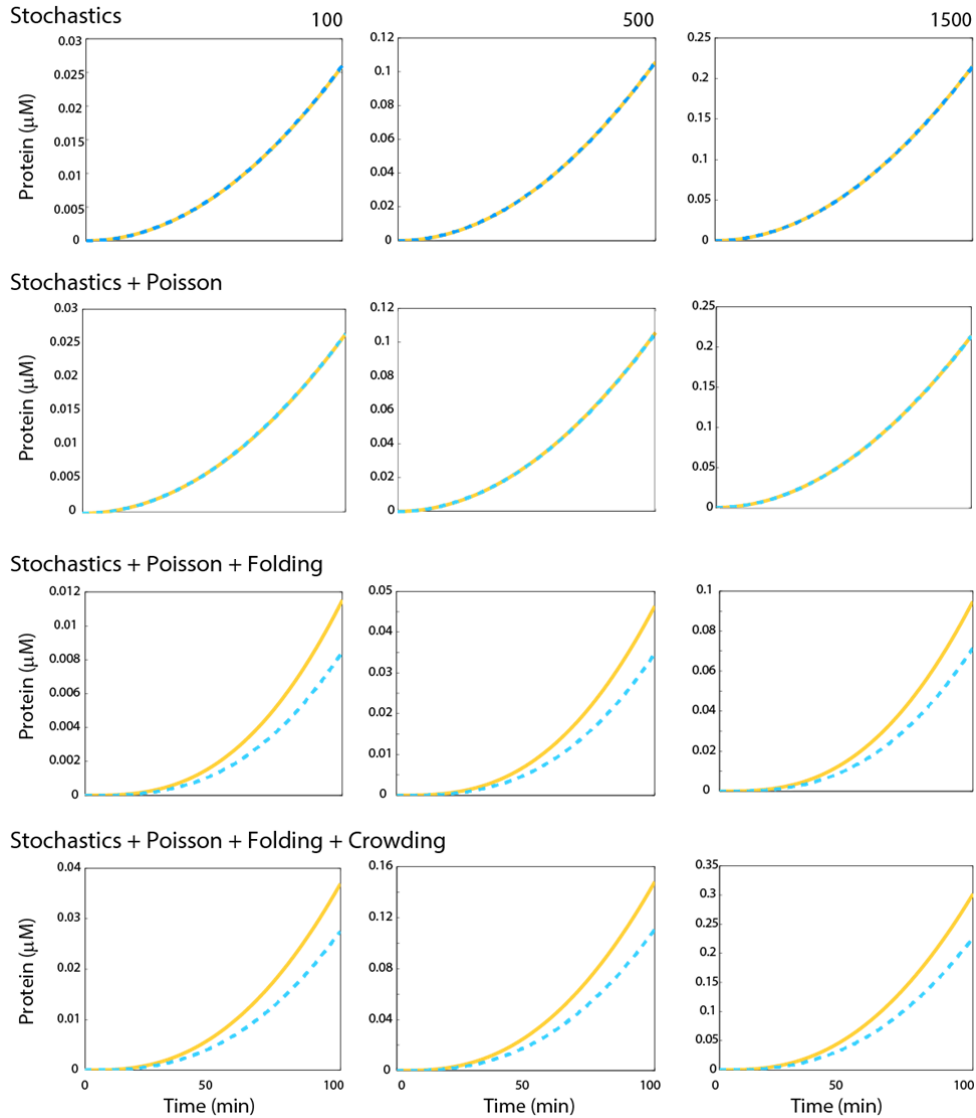
### *mRNA expression profiles*

Results of simulations using Gillespie's algorithm (Supplementary methods) showing mean mRNA transcription profiles for CFP and YFP over 200 iterations (representing 200 droplets) for different copy numbers (columns) and different factors incorporated in the model (rows).



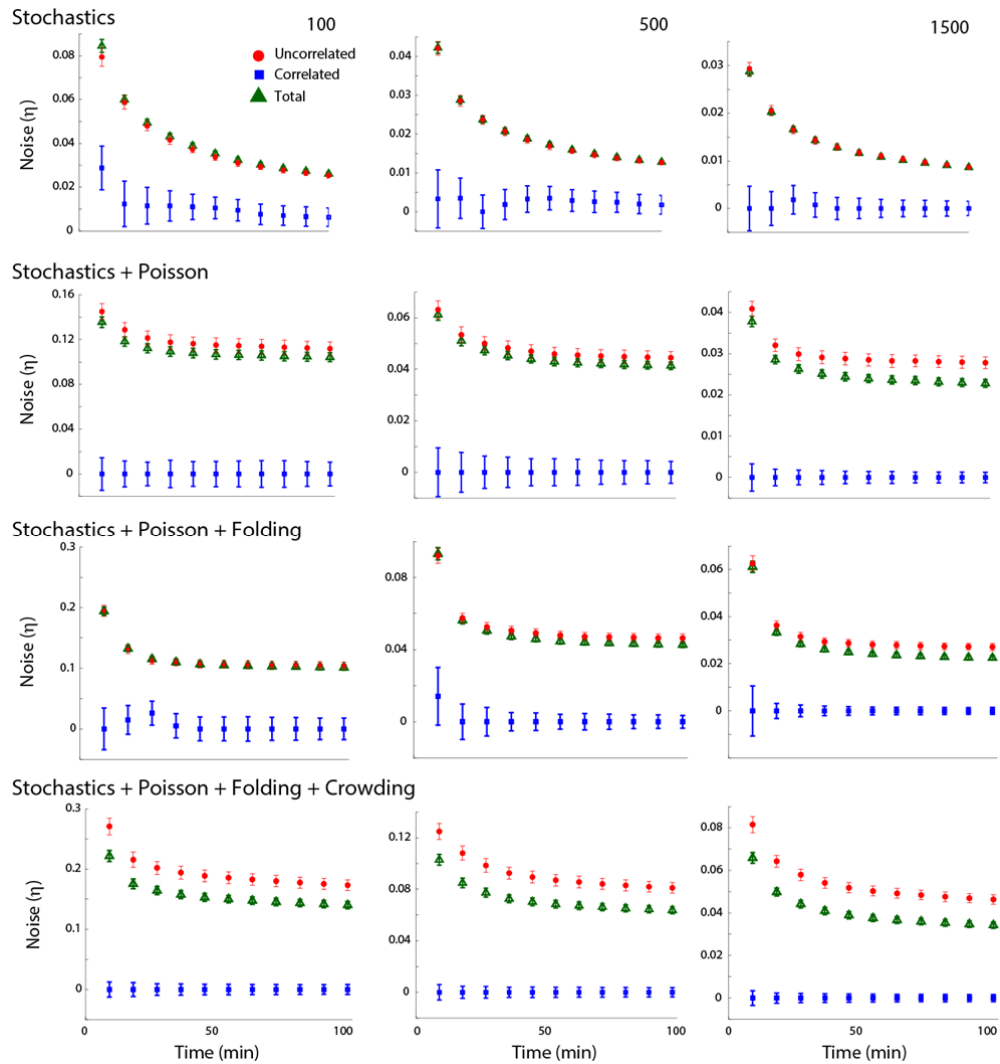
### Protein expression profiles

Results of simulations using Gillespie's algorithm (Supplementary methods) showing mean protein expression profiles for CFP and YFP over 200 iterations (representing 200 droplets) for different copy numbers (columns) and different factors incorporated in the model (rows).



### Noise profiles

Analysis of results from stochastic simulations using Gillespie's algorithm (Supplementary methods) as done for the experimental data gives noise over time for different copy numbers (columns) and different factors incorporated in the model (rows).

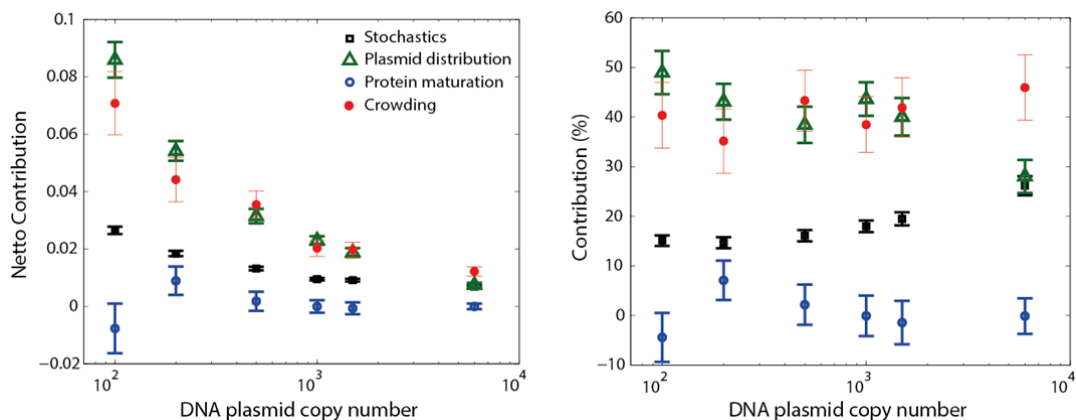


### Contribution of different factors to uncorrelated noise

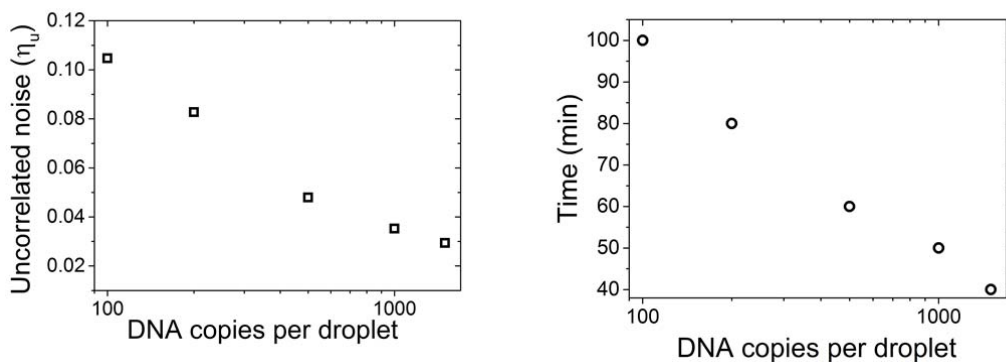
To quantify the effect of the different factors (stochasticity of biomolecular reactions, Poisson distribution of DNA plasmids, folding of proteins and crowding) on the uncorrelated noise both the netto contribution and percentage contribution of each factor was calculated at 100 minutes for different copy numbers. The netto contribution was calculated as follow:

- Netto contribution stochastics of reactions = uncorrelated noise stochastics
- Netto contribution poisson distribution of plasmids = (uncorrelated noise stochastics + poisson) – (uncorrelated noise stochastics)
- Netto contribution protein folding = (uncorrelated noise stochastics + poisson + folding) – (uncorrelated noise stochastics + poisson)
- Netto contribution crowding = (uncorrelated noise stochastics + folding + poisson + crowding) – (uncorrelated noise stochastics + folding + poisson)

The contribution in percentage was calculated with respect to the uncorrelated noise from simulations including all factors, i.e. stochastics of reactions, Poisson distribution of plasmids, protein folding and crowding.



**Supplementary Fig. 22**



For the dilute stochastic simulation (including Poisson distribution of plasmids and folding of CFP and YFP) we found time points where the amount of protein produced was the same (about  $0.03 \mu\text{M}$ ) and plotted the uncorrelated noise values (on the left) at these time points (shown on the right). This shows exactly the same trend as the uncorrelated noise values at 100 minutes after the start of expression. Therefore the trend of uncorrelated noise over plasmid copy number is caused by a combination of the Poisson distribution of plasmids and the stochastic nature of protein expression and not by higher or lower amounts of proteins produced.

## **Supplementary methods**

### ***Image analysis***

Fluorescence was measured every ten minutes for approximately three hours using a fluorescence microscope. The images were analysed using a Matlab program. At least 200 droplets were used for the analysis. For every time point the same procedure was followed. Droplet and background detection were done using separate thresholds for the intensity, which were set manually for each time-point. Choosing the threshold for the background was done in a way to be sure no pixels from the droplets were taken as background. The threshold for the droplets was chosen in a way to be sure no background pixels were taken as droplets. Background subtraction was done by subtracting the mean intensity of the background pixels from the raw image. Furthermore, objects in the image smaller than the amount of pixels for a droplet (e.g. caused by dust) were removed. Then, for each time-point the procedure from Elowitz and co-workers was followed<sup>3</sup>. For each droplet the mean intensity of all pixels was calculated. Then, the mean intensity of each droplet was normalised by the mean intensity of all droplets. This was done for both CFP and YFP and the normalised intensities were plotted against each other. From this graph the uncorrelated ( $\eta_u$ ), correlated ( $\eta_c$ ) and total noise can be calculated according:

$$\eta_c^2 \equiv \frac{\langle I_{CFP} \cdot I_{YFP} \rangle - \langle I_{CFP} \rangle \langle I_{YFP} \rangle}{\langle I_{CFP} \rangle \langle I_{YFP} \rangle}$$

$$\eta_u^2 \equiv \frac{\langle (I_{CFP} - I_{YFP})^2 \rangle}{2 \langle I_{CFP} \rangle \langle I_{YFP} \rangle}$$

$$\eta_{tot}^2 \equiv \frac{\langle I_{CFP}^2 + I_{YFP}^2 \rangle - 2 \langle I_{CFP} \rangle \langle I_{YFP} \rangle}{2 \langle I_{CFP} \rangle \langle I_{YFP} \rangle}$$

Here  $I_{CFP}$  and  $I_{YFP}$  are the mean normalised intensities of CFP and YFP respectively of one droplet. Angled brackets indicate means over the cell population.

### ***Isolation and labelling of Alexa 647 labelled Ribosomes***

The labelling protocol was adapted from Blanchard and co-workers<sup>4</sup>. 5  $\mu$ M of ribosomes were incubated with 100  $\mu$ M NHS-Alexa 647 in 50 mM Tris-HCl pH 7.6, 15 mM MgCl<sub>2</sub>, 100 mM NH<sub>4</sub>Cl, 6 mM  $\beta$ -mercaptoethanol. Excess dye was washed using centricon 3000 spin columns (Merck Millipore, USA) with 100  $\mu$ M NHS-Alexa 647 in 50 mM Tris-HCl pH 7.6, 15 mM MgCl<sub>2</sub>, 100 mM NH<sub>4</sub>Cl, 6 mM  $\beta$ -mercaptoethanol. Subsequently the ribosomes were concentrated with Vivaspin 4 spin columns (Sartorius).

### ***Determining protein maturation times***

CFP and YFP were expressed using the standard cell free expression procedure described in the manuscript. When the mid expression phase was reached chloramphenicol (2.8  $\mu$ g  $\mu$ L<sup>-1</sup>) was added



to block translation. Therefore any additional fluorescence arising after this point is due to additional protein maturation and not production.

To calculate the maturation time, the increase in fluorescence after the addition of chloramphenicol was normalised from 0 to 1, and the maturation time was described as the time at which 63% of the fluorescence intensity was reached<sup>5</sup>.

### ***Fluorescent recovery after photobleaching***

Fluorescent recovery after photobleaching experiments were performed on an Olympus IX81 confocal microscope, with an Andor iXon3 camera, Andor 400-series solid state lasers, a Yokogawa CSU-X1 spinning disk and an Andor FRAPPA photobleach module. Droplets were made of a 1.6  $\mu\text{M}$  ribosome solution of which 29% was labelled with a NHS-Alexa 647 fluorophore. A 12  $\mu\text{m}$  strip was bleached at 100% laser intensity ( $\lambda = 637 \text{ nm}$ , dwelling time 200  $\mu\text{s}$ , 2 repeats). Fluorescent recovery was subsequently monitored ( $\lambda = 637 \text{ nm}$ , exposure time = 200ms, Gain = 300).

For the fluorescent recovery the raw data was normalised after auto-fluorescence subtraction, using the following equations.

$$I_{\text{frap-norm}}(t) = \frac{I_{\text{drop-pre}}}{I_{\text{drop}}(t) - I_{\text{background}}(t)} \cdot \frac{I_{\text{frap}}(t) - I_{\text{background}}(t)}{I_{\text{frap-pre}}}$$

Where  $I_{\text{drop-pre}}$  is the intensity of the droplet before bleaching,  $I_{\text{drop}}$  is the intensity of the droplet,  $I_{\text{background}}$  is the background fluorescent intensity,  $I_{\text{frap}}$  is the fluorescent intensity of the frap region and  $I_{\text{frap-pre}}$  is the intensity of the frap region before bleaching.

The diffusion coefficients were subsequently computed using Ellenbergs diffusion fitting.

$$I(t) = I_{\text{final}} \left( 1 - \left( \frac{w^2}{w^2 + 4\pi Dt} \right)^{1/2} \right)$$

Where  $I_{\text{final}}$  and  $D$  are computed parameters,  $I_{\text{final}}$  is the mobile fraction and  $D$  the diffusion coefficient.

The fitting of the Diffusion coefficients in Fig. 4a is based on Stokes' law for the diffusion coefficient  $D \sim 1/\mu$ , with  $\mu$  being the viscosity of Ficoll (GE Healthcare Data File 18-1158-27-AB).

### ***In vitro transcription***

The transcription only reaction buffer consisted of 50 mM Hepes with pH 8.0, 2.4 mM Guanosine Triphosphate (GTP), 1 mM Adenosine Triphosphate (ATP) and Cytidine Triphosphate (CTP) and Uridine Triphosphate (UTP) each, 0.66 mM Spermidine, 0.5 mM cyclic adenosine monophosphate (cAMP), 0.22 mM Nicotinamide adenine dinucleotide (NAD), 0.17 mM coenzyme A, 20 mM 3-phosphoglyceric acid (3-PGA), 0.045 mM folinic acid, 0.13  $\text{mg mL}^{-1}$  transfer ribonucleic acid (tRNA), 1 mM of each amino acid, 10 mM magnesium glutamate, and 86 mM potassium glutamate, T7 RNA polymerase (130 U), 0.5  $\mu\text{M}$  Molecular beacon.

### **Construction of 32 x BT**

An overview of the method of construction is shown in supporting Fig. 4 and is based on the method described by Robinett and co-workers<sup>6</sup>. The following oligonucleotide and its complimentary strand were ordered from Integrated DNA Technologies:

```
ATCGGTCGACCTTACCCTTAAATTTATTTGCGTACGCCATAGCTAGCTACACTTACC  
CTTAAATTTATTTGCAACGTACCTAACGCATCGACTTACCCTTAAATTTATTTGCTA  
CTATACTAAACTACCTACTTACCCTTAAATTTATTTGCACTACTGGAAAACCTACCTC  
TCGAGGGACTGATCACTTGGGATCCATG
```

This was combined with its complementary oligonucleotide and which was cut and inserted into pUC18 vector (thermo Scientific) with *Sall* and *BamHI*. Sequential doublings of this sequence were performed as shown in Fig S14. Subsequently the 32 repeat sequences was inserted into pET-28a-c(+) vector (Novagen) using *HindII* and *XhoI*.

### **Molecular beacon sequence**

The backbone of the molecular beacon was composed of 2'-O-methylribonucleotides. The molecular beacon was synthesized by Integrated DNA Technologies (optical density at 260 nm = 5.3), resuspended in autoclaved Milli-Q water to a concentration of 50  $\mu$ M and stored in light protected tubes at -20°C.

```
/5Alex488N/mCmCmGmCmAmAmAmUmAmAmUmUmUmAmAmGmGmGmUmAmAmGmCmGm  
G/3IABkFQ/
```

### **Imaging and analysis of mRNA expression**

Confocal microscopy imaging was performed with an Olympus IX81 confocal microscope with an Andor iXon3 camera, Andor 400-series solid-state lasers, and a Yokogawa CSU-X1 spinning disk unit ( $\lambda$  = 488 nm, exposure time = 800ms, Gain = 300).

Images corresponding to Fig. 5 b, c, d and Fig S15 were taken using 10 focal planes over 18  $\mu$ m covering the whole droplet (of approximately 10  $\mu$ m high). A maximum intensity Z-projection was generated using only the focal planes covering the droplet. After rolling ball background subtraction, a threshold value was determined for all images. The number of particles above this threshold intensity were analysed in ImageJ, per droplet per time interval and the particles which were between 3-30 pixels were counted.

For Fig. 5 c the average fluorescent intensity per droplet of all spots were measured, and the average fluorescent intensity of the whole droplet. For both, background and blank were subtracted.

### **Modelling of mRNA localisation**

To model the mRNA accumulation we used Michaelis Menten kinetics to determine the effective rate of transcription ( $V$ ) of one plasmid:

$$V = \frac{V_{max} \cdot S}{K_m + S}$$

Here  $V_{max}$  and  $K_m$  ( $V_{max} \text{ max} = 722.64 \text{ mRNA min}^{-1}$  and  $K_m = 3613.2 \text{ DNA plasmids}$ ) were previously determined (Fig. 17) and the substrate concentration (S) was set at 1. Therefore we could determine the production of one mRNA (in  $\text{s}^{-1}$ )

We took the calculated diffusion coefficients of polysomes (Fig. 18) and defined the distance (x) the polysomal complex needed to diffuse to generate a homogeneous environment as half the distance between two plasmids ( $\pm 3 \mu\text{m}$ ).

$$t_{\text{Diff}} = \frac{x^2}{6D}$$

### **Stochastic Gillespie algorithm**

The stochastic cell free gene expression in 200 droplets was simulated using Gillespie's Direct Method algorithm. The theoretical model describes transcription and translation as single step reactions each with a different probability based on the corresponding reaction rates which are calculated using Michaelis-Menten kinetics including substrate competition .

$$V = \frac{V_{max} \cdot [S]}{K_m \left(1 + \frac{[I]}{K_m}\right) + [S]} \quad \text{with} \quad V_{max} = k_{cat} \cdot [E]$$

Here  $V_{max}$  again is the maximum rate at which the total amount of enzyme in a droplet performs. The competitive substrate is indicated by [I]. We determined the  $V_{max}$  and  $K_m$  of polymerase by fitting experimental data (Fig. 17) ( $V_{max} \text{ max} = 722.64 \text{ mRNA min}^{-1}$  and  $K_m = 3613.2 \text{ DNA plasmids}$ ). Post-translational folding of CFP and YFP was described using first-order rates which were experimentally obtained (Fig. 18). The Michaelis-Menten parameter for the ribosome was calculated ( $K_m = 4.3573\text{e}5 \text{ mRNA}$ ) using values previously determined by Stögbauer and co-workers<sup>7</sup>. The  $V_{max}$  of the ribosome was determined by fitting the experimental data of protein expression in dilute environment with a plasmid copy number of 7600, using the stochastic Gillespie algorithm. which included transcription, translation and protein maturation.

Simulations were performed for a range of plasmid copy numbers from 10 – 1500 copy numbers. For each plasmid copy number 200 iterations (representing 200 droplets) were performed from which the noise values were calculated in the same way as for the experimental data. Furthermore, the amount of enzymes was kept constant over the iterations. To analyse and visualize the different contributions to uncorrelated noise of the stochastics of transcription and translation, protein folding, Poisson distribution of the CFP and YFP plasmids and crowding simulations were performed by adding one by one each of these factors. First, simulations were performed describing transcription and translation starting with the same plasmid copy number for CFP and YFP production over the 200 iterations. Subsequently, protein folding, Poisson distribution of CFP and YFP copy numbers over the 200 iterations and crowding were included in the model. Simulating the crowded environment was done by using a 10 times higher probability for a ribosome to rebind to the same mRNA (p.n-1), which accounts for the localisation of the mRNA at the production point, resulting in a heterogeneous distribution of the polysomal complexes creating. This creates local microenvironments of high concentrations of biologically active machinery, where the machinery has a higher probability of rebinding.

1. Brandt, F. et al. The Native 3D Organization of Bacterial Polysomes. *Cell* **136**, 261-271 (2009).
2. Svergun, D.I. & Nierhaus, K.H. A Map of Protein-rRNA Distribution in the 70 S Escherichia coli Ribosome. *Journal of Biological Chemistry* **275**, 14432-14439 (2000).
3. Swain, P.S., Elowitz, M.B. & Siggia, E.D. Intrinsic and extrinsic contributions to stochasticity in gene expression. *Proceedings of the National Academy of Sciences* **99**, 12795-12800 (2002).
4. Blanchard, S.C., Kim, H.D., Gonzalez, R.L., Puglisi, J.D. & Chu, S. tRNA dynamics on the ribosome during translation. *Proceedings of the National Academy of Sciences of the United States of America* **101**, 12893-12898 (2004).
5. Hebisch, E., Knebel, J., Landsberg, J., Frey, E. & Leisner, M. High Variation of Fluorescence Protein Maturation Times in Closely Related Escherichia coli Strains. *PLoS ONE* **8**, e75991 (2013).
6. Robinett, C.C. et al. In vivo localization of DNA sequences and visualization of large-scale chromatin organization using lac operator/repressor recognition. *The Journal of cell biology* **135**, 1685-1700 (1996).
7. Stogbauer, T., Windhager, L., Zimmer, R. & Radler, J.O. Experiment and mathematical modeling of gene expression dynamics in a cell-free system. *Integrative Biology* **4**, 494-501 (2012).